Stereo Perception in the Dark using Uncalibrated Line Laser*

Srinivasan Vijayarangan[1] and David Wettergreen

***Abstract*— Perception using stereo requires external light. In the absence of natural light, active, structured light provides light where it is needed. In this work, we demonstrate how a free moving line striping laser can be used to perceive and model terrains. In this formulation, we do not need to know the position of the laser with respect to the stereo pair which precludes the need for calibrating the laser position. This also saves an actuator as the laser can be passively articulated using a spring. In this paper, we present the algorithms to efficiently extract the laser pixels from the stereo image pair. We also present techniques to use the structure of the light and overcome degenerate cases to build cleaner maps. This perception method benefits micro-rovers specifically those trying to operate in the extreme lighting conditions.**

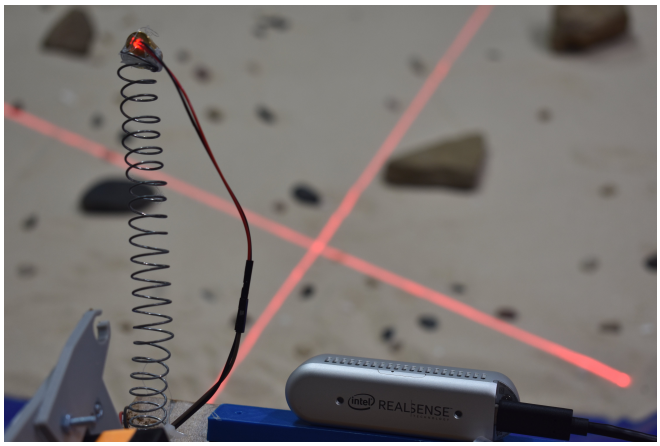


Fig. 1. Passively articulated crosshair laser mounted on a spring

I. INTRODUCTION

To explore an environment effectively, a map is needed to aid in navigation and localization and as a product itself. NASA's Lunar Surface Instrument and Technology Payloads (LSITP) program is supporting development of small rovers, weighing less than 20 kilograms, called micro-rovers, to explore the Moon. Particularly, when exploring a planetary surface like the lunar poles where no human or robot has ever landed, mapping becomes crucial. Micro-rovers are not new. Sojourner [1] is one of the early micro-rovers which weighted only 11.5 kgs. More recently the Pragyan [2] rover from the Chandrayaan 2 mission also falls on gamut of mirco-rovers. MoonRanger [3] is one of the new breed of rovers and will be flying to the Moon in December 2022. Recent developments in computing and sensing has made these machines quite capable and hence the renewed interest. For these rovers to survive, they need to exhibit complete autonomy including navigation. Perceiving the terrain is an important first step for navigation.

For terrestrial perception applications, LiDAR have become ubiquitous. However they are fragile for space applications which have severe launch vibrations and thermal and radiation extremes. Recently flash LiDARs like DragonEye [4] have gained prominence as they do not have any moving parts and have flown in space. LiDAR are also bulky and costly for a micro-rover. The cheaper commercially available units like Picoflexx [5] are lighter but have very low resolution. An alternate option is to use stereo cameras, which are lighter with no moving parts and have proven space legacy. However they need external light source. Kyle and Liam [6] studied using a strobe light and more recently MacTavish et al. [7] looked at the effects of passive lights on visual odometry which is not a viable option for micro-rovers due to power and heat concerns. Selectively illuminating the scene using active light source is a better alternative. Grunnet-Jepsen, et.al., [8] accomplish this by projecting random dots which both illuminate the scene and provide additional texture. However since the light is dispersed to a larger area, this method works indoors or in low light. Structured light solutions like laser line stripers have been studied for decades [10] in the context of mapping. In this paper, we will focus on structured light sensors like line stripers in the context of micro-rover mapping and explore methods to exploit inherent structure in the light source. The rest of the paper is structured as follows. Section II studies prior work, followed by the approach in Section III where the algorithms and procedures are discussed. In Section IV experiments and results are discussed followed by conclusions and future work in Section V.

II. PRIOR WORK

The digital Michelangelo project [9] is the seminal work on using line striping for reconstruction. Levoy et al. demonstrated a high accuracy pipeline using line stripers and cameras to do dense reconstructions on a large scale. Line stripers have been studied for robotics application much earlier than that. The work by Escalera et al. [10] studied line striping for robot localization and terrain mapping by incrementally accumulating the laser lines. Line stripers have space heritage. The Sojourner micro-rover used line stripers [14] for hazard detection. Matthies et al. [11] extend the idea for terrain reconstruction and study parameters like aperture, wavelength and albedo that influence perception in both dark

*The technology, rover development and flight are supported by NASA LSITP contract 80MSFC20C0008 MoonRanger.

Authors are with Robotics Institute at Carnegie Mellon University, Pittsburgh, USA

[1]srinivasan@cmu.edu

and bright conditions. Jamal et.al. [12] assume negligible slip to successfully build a terrain model. However Maimone et al. [15] showed that slip is unavoidable and in some instances can be quite bad. One way to counter this problem, is to project multiple lines at the same time as shown by Massot-Campos et al. [16]. However, this disperses the laser power to multiple lines and hence makes it less visible in direct sunlight. Also, the complexity of the line extraction algorithm increases due to multiple lines in the image.

It is also possible to articulate the line striper. This has resemblance to LiDAR, but LiDAR has both the light source and the receiver internally which precludes any in-field calibration or extrinsic estimation. Typically the line striper is calibrated with respect to the cameras. We can however use the stereo cameras to extract the line striper extrinsics as shown in [17]. Takashi et al. [18] build a terrain model of underwater hydro thermal chimneys by panning the laser. The laser could also be spun along its optical axis and mounted inside the chassis as it only needs a single circular opening. However spinning the laser produces degenerate cases which will be discussed later in Section III. Typically, a monocular camera is used for line striping. However using a stereo camera setup provides the convenience of not needing to pre-calibrate the laser and also yields more accurate point clouds as shown by Inglis et al. in [21]. We use a similar stereo setup and extend the idea to employ a free moving line striping laser to perceive and model terrains. We present algorithms to efficiently extract the laser pixels from the stereo image pair and techniques to use the structure of the light and overcome degenerate cases to build cleaner maps. Our experimental results show this perception method benefits micro-rovers, specifically those trying to operate in the extreme lighting conditions. To our knowledge, this is a novel formulation for this application.

III. APPROACH

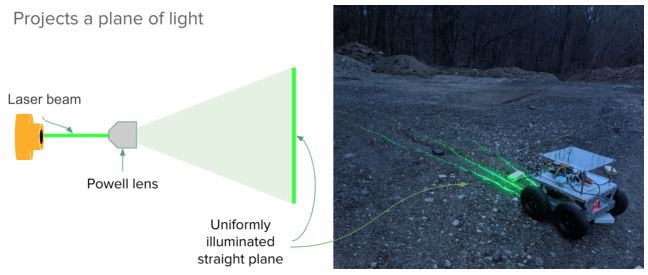


Fig. 2. (left) Basic operation of a line striping laser (right) Prototype rover employing three line striping lasers

The basic operation of a line striper is shown in figure 2. A laser diode projects a laser beam typically less than 3mm in diameter through a Powell lens. The Powell lens produces a sheet of light which, when intersecting with the terrain, becomes a line or a contour that follows the shape of the terrain. Since the laser is projected as a plane, the extracted 3D points can be constrained to a plane (there by using the structural information) to construct a cleaner terrain map. Jamal et.al. [12] detail the mapping process using fixed line stripers. In the typical single camera setup, the laser plane equation is estimated as a part of the calibration procedure [13]. The intersection of the rays from the camera origin, through the pixels, to the laser plane gives the position of the 3D points. In the stereo camera setup [17], epipolar geometry is used to calculate the position of the 3D points. In this case the laser plane equation is not estimated directly.

A. Articulated Line Striping

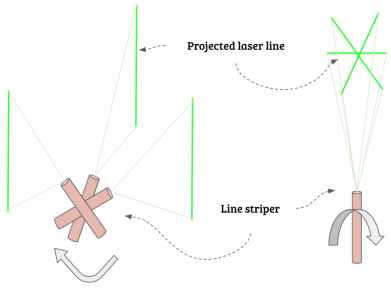


Fig. 3. (Left) Line striper articulated along the orthogonal axis (panner) (Right) Line striper articulated along the optical axis (spinner)

Algorithm 1: Accumulate Terrain Map

Result: $Ptcloud := N \times 3 points$
Set the distortion D^l, D^r, stereo rectification R^l_{rect}, R^l_{rect}, focal length f, baseline $baseline$ parameters from stereo calibration;
for *every angle increment of the line striper* **do**
  Get left and right images I^l and I^r;
  $uI^l := Undistort(D^l, I^l)$;
  $uI^r := Undistort(D^r, I^r)$;
  $sI^l, sI^r := StereoRectify(R^l_{rect}, R^l_{rect}, uI^l, uI^r)$;
  for *each row in* sI^l *and* sI^r **do**
    $disparity :=$
     $Bright(sI^l[row]) - Bright(sI^r[row])$;
    $Pt := Triangulate(disparity, f, baseline)$;
    $Ptcloud.append(Pt)$;
  end
end

The line striper can be articulated either along the optical axis (*spinner*) or along orthogonal axis (*panner*). Figure 3 shows a graphic of a spinner and panner setup and how the laser lines are accumulated. Each of these method have their own benefits. Algorithm 1 details the mapping process. First, a stereo image pair is acquired. The image pair is undistorted to correct for barrel/pin-cushion distortions and stereo rectified. Stereo rectification process applies a homography to the stereo image pair so that the epipolar lines are parallel and aligned. That is, for any pixel in the left image the corresponding pixel lies in the same rows of the right image. Disparity is calculated by extracting the location of the brightest pixels in each row of image

pair. Once the disparity is extracted, the 3D position of the point can be calculated using triangulation. These points are then accumulated to form the point cloud. This process is repeated after the laser is moved (panned or spun) in small angle increments. For an accurate map, the robot needs to be stationary or the accurate position of the robot needs to be known when mapping. The time feasibility of this method depends on the sensitivity of the camera sensor which in-turn dictates the shutter speed. In our experiments, we found a shutter speed of one to five milliseconds is sufficient. However the method also is flexible and the size of the map can be adjusted based on need. The accuracy of the generated map relies largely on the stereo calibration and the pixel extraction procedure (*Bright* method in algorithm 1). The pixel locations can be extracted using a naive thresholding approach where the intensity of each pixel is compared to a preset value. The first pixel that exceeds the preset value in each row is detected. Figure 4 shows the result using this method. The detected pixels are not in the center of the laser as this method just looks for the first bright pixel. Though this is a naïve method, it is fast and captures the coarse structure of the scene.

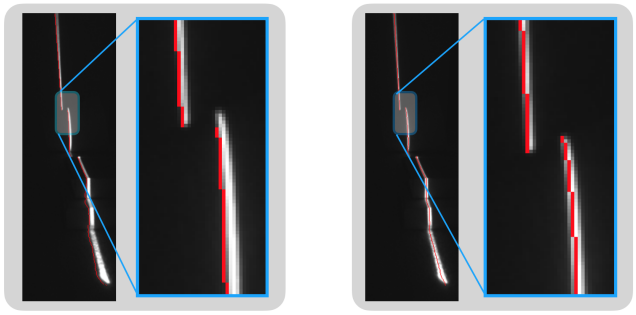


Fig. 4. (Left) Laser line extraction using the naïve method and (Right) the weighted average method. The white and grey pixels correspond to the laser whereas the red pixels correspond to the detections using this method

However this method can be improved using a weighted average approach where the weighted mean of the pixel intensities are used. For each row, the block of bright pixels are found and a simple weighted mean is applied where the pixel intensity forms the weights.

$$X_{mean} = \frac{\sum_{i=1}^{n} w_i X_i}{\sum_{i=1}^{n} w_i} \tag{1}$$

Here X_{mean} is the estimated pixel value and w_i is the intensity of the pixel at the i^{th} location and n is the total number of rows. This method produces sub-pixel locations. Figure 4 shows the result using the approach where the center pixels are detected along the laser line. Pixel extraction accuracy can further be improved by following some of the techniques mentioned by Scharstein and Szeliski in [19]. However this work focuses on the viability of the articulated line striping solution.

As mentioned in section II, the laser can either be panned [18] and spun along the optical axis. Panning the laser projects the laser plane perpendicular to the camera baseline. This aids in the disparity calculation as most of the pixel associations will have a valid disparity. The field-of-view of the scan can be controlled by limiting the start and end angles. This enables quick scanning instead of getting complete scans every time. Since the line striper rotates along the orthogonal axis, it is harder to mount the panner inside the chassis.

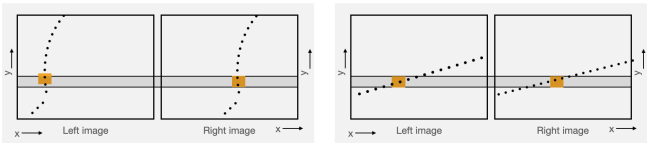


Fig. 5. Cartoon demonstrating the degenerate case that arises by spinning the laser. The grey bar show the matching epipolar line and the dotted line shows the profile of an object observed by the cameras. (Left) Normal case where the disparities can be extracted for each row. (Right) Degenerate case where the disparities are limited to a few rows.

A spinning laser can be fabricated to a small form factor as it spins about the optical axis and can be mounted inside the chassis of the rover. However, the laser plane is not always perpendicular to the camera baseline as in the case of the panning setup. Pixel depth estimation starts deteriorating as the laser plane becomes parallel to the camera baseline. This causes a degenerate case [20]. Figure 5 shows a cartoon of the left and right image from a stereo pair. When the orientation of the laser plane changes from vertical to horizontal, the disparities get squeezed to just a few rows and hence fewer 3D points. When the laser plane is horizontal all the pixels will lie on the epipolar line and hence no disparity can be calculated.

B. Uncalibrated Laser

Since micro-rover are limited by weight, it is beneficial to reduce the extra articulation for the laser.

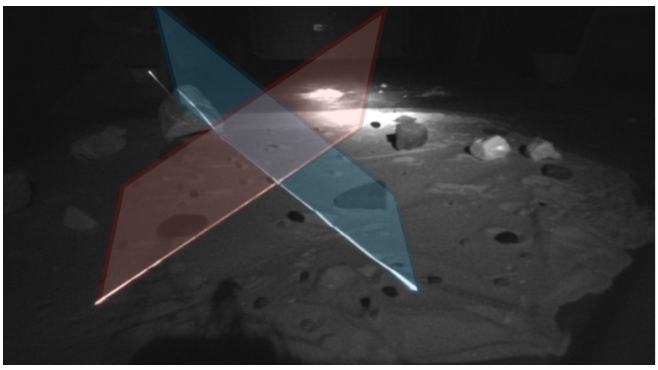


Fig. 6. A scene with two lines from a crosshair laser. The red and blue planes are the orthogonal planes projected by the crosshair laser.

We propose articulating the laser passively by mounting it on a spring and let it operate akin to a ”bobblehead”. In such a setup, we will not have much control on the orientation of projected laser line. The resulting orientation will not always be perpendicular to the baseline. We propose using a crosshair laser instead of a line laser to mitigate this problem.

A crosshair laser (Figure 6) projects two laser planes which are orthogonal. In this configuration, even if one plane is parallel to the baseline, the other is not and hence disparities can be calculated. The orthogonality of the laser planes can also be used as a constraint to refine the extracted 3D points. Compared to a line laser, the crosshair setup reduce the light intensity by dispersing to two lines. However it is minimal compared to the multi-line/dot projectors and the benefits outweigh the deficiency.

Since we are using a stereo setup we do not need to know the exact position of the laser at any point and hence can accommodate the passive articulation of the laser. This means one less actuator and the associated complexity that comes with the actuation. This means a huge win for a micro-rover as the resources are pretty limited. We draw inspiration from the Zebedee sensor [22]. Zlot and Bosse mounted an IMU and a 2D laser on a spring and formulated a method to estimate the position of the laser with help from an IMU. In contrast, the bobblehead laser does not need to know the position of the laser. On the Moon, the lack of atmosphere reduces the drag and hence helps the bobblehead to oscillate longer. Our main contribution in this work is to use bobblehead and crosshair lasers jointly which reduces the need for an additional actuator which helps the micro-rover resource constraints. The steps to extract the 3D points is identical to those noted in Algorithm 1.

1) Pixel Spread Factor: The bobblehead laser follows simple harmonic motion. This means that the velocity of the bobblehead rises and falls, regularly introducing motion blur at the faster sections. Estimating 3D points from an image with motion blur leads to noise as it violates the laser plane assumption. There are three ways we can address motion blur.

- choose a spring with desired harmonics
- set a low exposure time (fast shutter speed)
- detect and eliminate frames with motion blur

$$S = \frac{\sum_{i=1}^{n} (X_{end} - X_{start})}{n} \tag{2}$$

Shutter speed is influenced by the camera's sensitivity, intensity of the laser light and the look ahead distance. Frames with motion blur can be detected using the simple metric. We call it the pixel spread factor (S) (see Equation 2) which is given by mean of the differences between the start(X_{start}) and end location(X_{end}) of the bright pixels. Through experimentation we found a pixel spread factor of less than 8 detects frames with motion blur reliably.

After the pixels are detected in left-right pair separately, they are matched, the disparities are calculated and then triangulated to find the 3D position of the pixels. Since we are using stereo, we can use the epipolar geometry to find the disparities easily. The stereo rectification step makes sure that the epipolar lines are parallel and aligned to the image rows. So for each row, we can match the detected pixels from the left image to the right image.

2) Double-detections: Left frame of Figure 7 shows the matches from an image. Some unmatched (red pixels) are due to the second detection in the same row. This can happen because of the geometry of the scene. In the case of the cross hair laser it is unavoidable as there are two lines to detect.

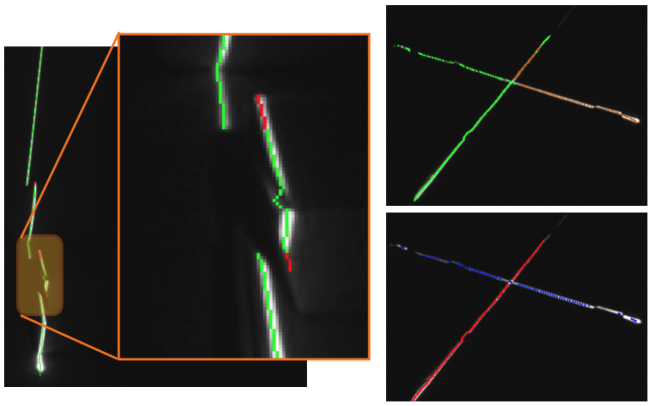


Fig. 7. (Left) Shows double detections problem. The gray and white pixels correspond to the laser line. The green and red points show the matched and unmatched pixels between the left and right images respectively. Some unmatched (red pixels) are due to second detections in the same row. (Top right) Shows the result of detecting multiple pixels in a row. The first detection is marked in green and the second detection is marked in orange. (Bottom right) Shows the result of the laser plane detection method. The red and blue dots correspond to single laser plane respectively

We can solve this problem by keeping track of the detections in each image and match the n'th detection in the left image to the corresponding n'th detection in the right image. Top right frame in Figure 7 shows the multiple detections. However the matching algorithm is not aware of the points corresponding to the laser plane and matches them blindly in the order they appear.

3) Laser Planes: Given that we are using structured light, it should be possible to exploit the structure of the light itself. The crosshair laser projects two orthogonal planes. After estimating the 3D points using the previous steps, the laser planes can be estimated using RANSAC [23]. Algorithm 2 and 3 detail the steps involved. The 3D points can then be filtered by ignoring the points which do not lie on the plane. This opens up possibilities as the detection threshold can be increased to allow more points to be evaluated and filtered later using the laser plane test. Bottom right frame of Figure 7 show the pixels from the orthogonal laser planes.

IV. EXPERIMENTS

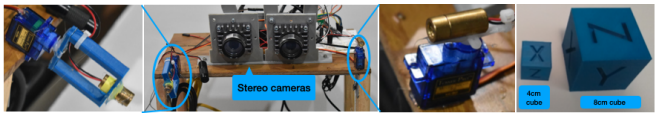


Fig. 8. (From left) The spinning laser, platform with the stereo cameras and the articulated lasers, the panning laser and calibration cubes used for stereo comparison

Figure 8 shows the experimental setup. For the panning and spinning laser setups, a stereo rig is used with two

Algorithm 2: RANSAC Laser Planes

Result: $[a, b, c, d]$, inliers, outliers
Set input point cloud *PtCloud*, *inlierThreshold*, *inlierPercent* ;
for *n iterations* **do**
  P^1, P^2, P^3, *RemainingPts* := Random(*PtCloud*);
  $[a, b, c, d]$:= FitPlane(P^1, P^2, P^3);
  inliers = [];
  outliers = [];
  for P^i *in RemainingPts* **do**
    d := DistanceToPlane($[a, b, c, d]$, P^i);
    if $d \leq inlierThreshold$ **then**
      inliers.append(P^i);
    else
      outliers.append(P^i);
    end
  end
  if $len(inliers) \geq inlierPercent$ **then**
    return $[a, b, c, d]$, inliers, outliers;
  end
end
return Error;

Algorithm 3: Estimate Laser Planes

Result: $[a_1, b_1, c_1, d_1]$, $[a_2, b_2, c_2, d_2]$
Set input point cloud *PtCloud* ;
$[a_1, b_1, c_1, d_1]$,-,$outliers_1$:= RANSACLaserPlanes(*PtCloud*);
$[a_2, b_2, c_2, d_2]$,-,- := RANSACLaserPlanes($outliers_1$);
return $[a_1, b_1, c_1, d_1]$, $[a_2, b_2, c_2, d_2]$

FLIR's BFS-PGE 2.3MP monochrome cameras tilted 20° from the horizontal axis, looking down. The cameras are connected to an Intel NUC via a GigE switch where the data is recorded. The lasers are mounted on hobby grade SG90 servos and controlled using an Arduino. The mounting parts are 3D printed. For crosshair-bobblehead laser setup, cameras from an Intel® RealSense™ D435 unit, tilted 20° from the horizontal axis, is used for stereo imagery (see Figure 1). The laser is rated at 50mW and operate at 3.3V. The laser is mounted on a spring attached closer to the cameras. The platform is pushed manually to excite the spring which happens naturally in a robot when it start/stops driving.

A. Natural Scene Reconstruction

To mimic a natural scene, a sandbox is setup with sand and rocks of different shapes and shades. First articulated lasers are setup to observe the scene, followed by the crosshair-bobblehead laser. The data is collected in complete darkness with just the light from the laser. Exposure time is set between one to five milliseconds.

1) Articulated Lasers: Figure 9 shows the point clouds generated using the articulated laser setups. Most of the rocks including the smaller ones show up in the scan. Notice the

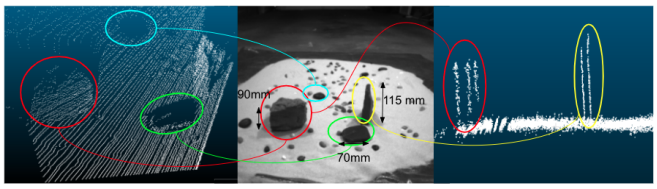


Fig. 9. (From left) Point cloud generated using the spinning laser setup, mock natural scene with playsand and rocks, point cloud generated using the panning laser

darker rock in the front appears mostly as a hole in the spinning laser point cloud (first from left in Figure 9) as it absorbs most of the light. This can be mitigated either by increasing the laser power or adaptively choosing the pixel threshold. An important point to note is the accuracy of the point cloud does not depend on the accuracy of the articulation but rather on the accuracy of the stereo calibration. In fact, the angle of the laser is not considered for point cloud triangulation.

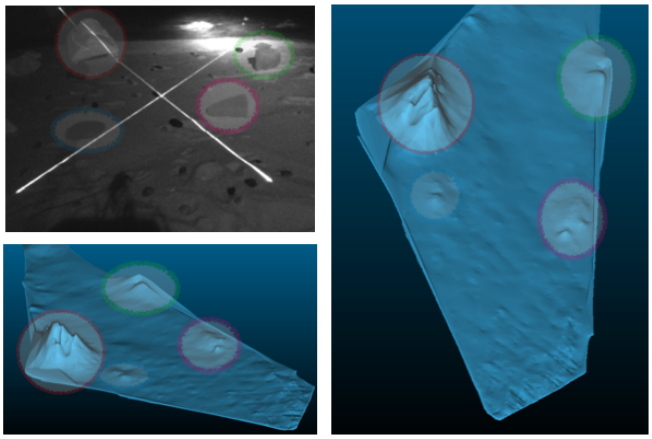


Fig. 10. Top left frame shows the natural scene mapped using the crosshair-bobblehead laser. Bottom left frame shows the side view of the mesh generated from the point cloud and the right frame shows the top view. Different objects are marked with different colors in the scene and matched with the corresponding colors in the mesh.

2) Crosshair-bobblehead Laser: Figure 10 shows the reconstruction of a similar natural scene. Instead of a point cloud, a mesh is shown for easy visualization. Similar to the articulated laser setup, the position of the laser is not tracked. The rocks show up proportional to their heights. Even the rocks with darker shade are represented in the mesh. This is because of the laser plane filtering algorithm which enables us to relax the pixel detection thresholds and evaluate more points which are later filtered during the laser plane test. This experiment demonstrates the feasibility of this method for terrain perception in the dark for a micro-rover setup.

B. Stereo Comparison

The next experiment compares the reconstructions from the crosshair-bobblehead laser and a stereo setup. For the stereo setup, Intel® RealSense™ D435 camera is used to precludes any algorithm tuning deficiencies. The onboard



Fig. 11. (From left) Calibration cubes with sides 4cm and 8cm, side view of the point cloud generated using the crosshair-bobblehead laser, side view of the point cloud generated using the RealSense™ camera

calibration procedure is run before the data collection. Since the experiment is conducted in total darkness, the IR dot projector on the RealSense™ unit is used for illumination. Calibration cubes of sides 4cm and 8cm are placed on a flat surface and data is collected. Figure 11 shows the result.

The crosshair-bobblehead laser reconstructs the planar surfaces of the cubes better than the RealSense™ camera. The sides of the cube are curvy and non-planar in the RealSense™ point cloud. The planar nature can be attributed to the extended baseline between the laser and the cameras, in the crosshair-bobblehead laser, as larger baseline generally leads to better triangulation. Closer inspection of the RealSense™ point cloud show divots on the ground plane which do not exist in the actual scene. These lead to incorrect maps which can be catastrophic for an autonomous rover making navigation decisions based off of these maps.

V. CONCLUSIONS

To summarize, we demonstrated that a free moving, untracked laser (line or crosshair) along with a stereo camera pair, can perceive and map an environment in complete darkness. First we discussed the procedure to extract 3D points from stereo images using an articulated line striping laser. Next we extended that approach to a passively articulated, untracked laser reducing the need for an extra actuator. Getting rid of an extra actuator also gets rid of the associated mounting and control circuitry and leads to reduced weight, power and thermal issues. This applies directly to micro-rovers as they are resource constrained systems and every gram counts. Particularly for the rovers like MoonRanger [3] intending to operate in the lunar polar region, perceiving in the dark becomes important. The crosshair-bobblehead laser solution provides a superior active lighting solution where the structure of the light is exploited to improve the mapping accuracy.

Future work will focus on improving the pixel extraction accuracy by adaptive thresholding the pixels; enforcing smoothness constraint on the extracted pixel by fitting a curve; and enforcing smoothness constraint across laser scans. Another potential venue is to formulate a procedure to arrive at the desired harmonic (which in turn affects the desired shutter speed) and coverage by altering the type of spring.

REFERENCES

[1] Wikipedia "Sojourner (rover)" https://en.wikipedia.org/wiki/ Sojourner_(rover), accessed on 11th Feb 2021.

[2] Wikipedia "Pragyan (rover)" https://en.wikipedia.org/wiki/ Pragyan_(rover), accessed on 23rd Feb 2021.

[3] "MoonRanger (rover)" https://www.cmu.edu/news/stories/archives/ 2020/september/moonranger-to-search-for-water.html, accessed on 23rd Feb 2021.

[4] Wikipedia "SpaceX Dragon" https://en.wikipedia.org/wiki/ SpaceX_Dragon, accessed on 29th Oct 2020.

[5] "Picoflexx" https://pmdtec.com/picofamily/wp-content/uploads/ 2018/03/PMD_DevKit_Brief_CB_pico_flexx_CE_V0218-1.pdf, accessed on 4th Mar 2021.

[6] Husmann, Kyle, and Liam Pedersen. "Strobe Lit High Dynamic Range Stereo Imagery for Dark Navigation"

[7] MacTavish, Kirk, Michael Paton, and Timothy D. Barfoot. "Night Rider: Visual Odometry Using Headlights." In 2017 14th Conference on Computer and Robot Vision (CRV), 314-20. Edmonton, AB: IEEE, 2017

[8] A. Grunnet-Jepsen, J.N. Sweetser, P. Winer, A. Takagi, J. Woodfill "Projectors for Intel® RealSense™ Depth Cameras D4xx" Accessed October 29, 2020 www.intelrealsense.com/wp-content/uploads/ 2019/03/WhitePaper_on_Projectors_for_RealSense_D4xx_1.0.pdf

[9] Levoy, Marc, Szymon Rusinkiewicz, Matt Ginzton, Jeremy Ginsberg, Kari Pulli, David Koller, Sean Anderson et al. "The Digital Michelangelo Project: 3D Scanning of Large Statues," 2000, 14.

[10] Escalera, A. De La, L. Moreno, M. A. Salichs, and J. M. Armingol. "Continuous Mobile Robot Localization by Using Structured Light and a Geometric Map." International Journal of Systems Science 27, no. 8 (August 1996): 771-82.

[11] Matthies, L., T. Balch, and B. Wilcox. "Fast Optical Hazard Detection for Planetary Rovers Using Multiple Spot Laser Triangulation." In Proceedings of International Conference on Robotics and Automation, 1:859-66. Albuquerque, NM, USA: IEEE, 1997.

[12] H.Jamal, V. Gupta, N. Khera, S. Vijayarangan, D. Wettergreen, W.L. Whittaker "Terrain Mapping and Pose Estimation for Polar Shadowed Regions of the Moon" International Symposium of Artificial Intelligence, Robotics and Automation in Space, October 2020.

[13] Zhou, F., & Zhang, G. "Complete calibration of a structured light stripe vision sensor through planar target of unknown orientations", Image and Vision Computing, (2005) 23(1), 59-67

[14] "Sojourner sensors" https://mars.nasa.gov/MPF/roverctrlnav/sensor.html accessed on 1st Mar 2021.

[15] Maimone, Mark, Yang Cheng, and Larry Matthies. "Two Years of Visual Odometry on the Mars Exploration Rove et al.rs." Journal of Field Robotics 24, no. 3 (March 2007): 169-86.

[16] Massot-Campos, Miquel, and Gabriel Oliver-Codina. "Underwater Laser-Based Structured Light System for One-Shot 3D Reconstruction." In IEEE SENSORS 2014 Proceedings, 1138-41. Valencia, Spain: IEEE, 2014.

[17] Gabrielle Inglis, Clara Smart, Ian Vaughn, Chris Roman, "A pipeline for structured light bathymetric mapping", IEEE/RSJ International Conference on Intelligent Robots and Systems, October 2012.

[18] Nakatani, Takeshi, Shuhao Li, Tamaki Ura, Adrian Bodenmann, and Takashi Sakamaki. "3D Visual Modeling of Hydrothermal Chimneys Using a Rotary Laser Scanning System." In 2011 IEEE Symposium on Underwater Technology and Workshop on Scientific Use of Submarine Cables and Related Technologies, 1-5. Tokyo, Japan: IEEE, 2011.

[19] Daniel Scharstein, Richard Szeliski, "High-Accuracy Stereo Depth Maps Using Structured Light", IEEE Computer Society Conference on Computer Vision and Pattern Recognition (CVPR 2003), volume 1, pages 195–202, Madison, WI, June 2003

[20] Srinivasan Vijayarangan, and David Wettergreen, "Verification of Stereo Camera Calibration Using Laser Stripers for a Lunar Micro-Rover", International Symposium of Artificial Intelligence, Robotics and Automation in Space, October 2020.

[21] Inglis, Gabrielle, Clara Smart, Ian Vaughn, and Chris Roman. "A Pipeline for Structured Light Bathymetric Mapping." In 2012 IEEE/RSJ International Conference on Intelligent Robots and Systems, 4425-32. Vilamoura-Algarve, Portugal: IEEE, 2012.

[22] Bosse, M., R. Zlot, and P. Flick. "Zebedee: Design of a Spring-Mounted 3-D Range Sensor with Application to Mobile Mapping." IEEE Transactions on Robotics 28, no. 5 (October 2012): 1104-19.

[23] Fischler MA, Bolles RC. Random sample consensus: a paradigm for model fitting with applications to image analysis and automated cartography. Communications of the ACM. 1981 Jun 1-24(6):381-95.